stand for several hours in a buffer solution at pH 6.4. The initial cyclic voltammetric response of the coating in the absence of substrate is also restored to its initial state. The catalytic activity can be recovered somewhat more rapidly at lower pH values, but we found no conditions where the restoration rate was close enough to the rate of catalyst degradation to prevent the loss of activity of the catalyst.

Conclusions

The slow chemical transformation that converts Ru(trpy)(bpy)$(OH)^{2+}$ from an unoxidizable into an oxidizable form has been argued to involve the replacement of a Ru(III)-terpyridine bond with a Ru(III)-OH_2 or Ru(III)-OH bond. Both the disproportionation of the Ru(III) complex and reversible proton-transfer reactions were ruled out as reactions that limit the rate of the transformation. Ru(trpy)(bpy)$(OH)^{2+}$ incorporated in Nafion coatings on graphite electrodes produces very stable electrochemical responses that persist for many days in the absence of oxidizable substrates. The latter undergo catalytic electrooxidations at the coated electrodes, but the catalyst is gradually degraded until it loses its activity after about 150 turnovers. Catalyst activity can be restored, but conditions where it remained active for extended periods could not be found. Nafion coatings appear more attractive than previously examined polymers as a means for holding highly oxidizing complexes on electrode surfaces.

Acknowledgment. This work was supported by the Dow Chemical Co. Dr. Mark Bowers was the source of considerable useful advice and indispensable computational assistance. Discussions with Prof. T. J. Meyer during the early stages of this work were also helpful.

Registry No. [Ru(trpy)(bpy)(OH_2)]$(ClO_4)_2$, 16389-43-8; Ru(trpy)(bpy)$(OH_2)^{3+}$, 89463-61-6; Ru(trpy)(bpy)$(OH_2)^{2+}$, 20154-63-6; Ru(trpy)(bpy)$(OH)^{2+}$, 81971-63-3; Ru(trpy)(bpy)$(O)^{2+}$, 73836-44-9; OH^-, 14280-30-9; HSO_4^-, 14996-02-2; N, 7727-37-9; Ru, 7440-18-8; Nafion, 39464-59-0; graphite, 7782-42-5; benzyl alcohol, 100-51-6.

Contribution from the Department of Chemistry, University of Houston, Houston, Texas 77004

Electrochemistry of the μ-Carbido Iron Tetraphenylporphyrin Dimer, $((TPP)Fe)_2C$, in Nonaqueous Media. Evidence for Axial Ligation by Pyridine

D. LANÇON and K. M. KADISH*

Received January 13, 1984

The electron-transfer reactions of the μ-carbido iron tetraphenylporphyrin dimer, $((TPP)Fe)_2C$, were investigated by electrochemical and spectroscopic techniques. In CH_2Cl_2 two reductions and four oxidations were observed between -1.90 and +1.60 V vs. SCE. All reactions involved single-electron-transfer steps and were reversible on the cyclic voltammetry time scale. Addition of pyridine to oxidized and reduced solutions of $((TPP)Fe)_2C$ indicated the formation of both mono and bis adducts. Values of log β_2 ranged between 7.7 ± 0.4 for $[((TPP)Fe)_2C(py)_2]^{2+}$ formation and 2.6 ± 0.4 for formation of $((TPP)Fe)_2C(py)_2$. A weak interaction of pyridine was also observed with $[((TPP)Fe)_2C]^-$. An overall oxidation-reduction mechanism is given in CH_2Cl_2/pyridine mixtures, and comparisons are made with ligand-binding properties of neutral and oxidized $((TPP)Fe)_2N$ and $((TPP)Fe)_2O$.

Introduction

Two iron porphyrins may be linked through a single bridging atom X:

$$(P)Fe-X-Fe(P)$$

where P = porphyrin and X = O, N, or C.[1] Most characterizations of these iron porphyrin dimers have involved μ-oxo complexes.[2] However, during recent years the structural and physicochemical properties of μ-nitrido[3-12] and μ-carbido[12-16] dimers have also generated considerable interest, especially in regard to the oxidation-state assignment of the iron center. The formal oxidation state is +3.5 for the $((TPP)Fe)_2N$ complex and +4 for the $((TPP)Fe)_2C$ species, but neither of these assignments is unambiguous, given the existing spectroscopic data. Also, for the diamagnetic μ-carbido dimer two resonance structures are possible:[1]

$$(P)Fe^{IV}=C=Fe^{IV}(P) \rightleftarrows (P)Fe^{II}\leftarrow:C:\rightarrow Fe^{II}(P)$$

The formalism of divalent iron best fits the solution spectroscopic data but does not agree with the Mössbauer spectra, which clearly indicate Fe(IV) at 131 K.[16]

Our own interest is in the redox properties and spectroscopic characterization of oxidized and reduced μ-oxo,[6,17,18] μ-ni-

(1) Smith, P. D.; James, B. R.; Dolphin, D. H. *Coord. Chem. Rev.* **1981**, *39*, 31.
(2) See for example: "The Porphyrins"; Dolphin, D., Ed.; Academic Press: New York, 1979; Vols. I-VII.
(3) Scheidt, W. R.; Summerville, D. A.; Cohen, I. A. *J. Am. Chem. Soc.* **1976**, *98*, 6623.
(4) Cohen, I. A. *Struct. Bonding (Berlin)* **1980**, *40*, 1.
(5) Schick, G. A.; Bocian, D. F. *J. Am. Chem. Soc.* **1980**, *102*, 7982.
(6) Kadish, K. M.; Cheng, J. S.; Cohen, I. A.; Summerville, D. A. *ACS Symp. Ser.* **1977**, *No. 38*, 65.
(7) Kadish, K. M.; Rhodes, R. K.; Bottomley, L. A.; Goff, H. M. *Inorg. Chem.* **1981**, *20*, 3195.
(8) Kadish, K. M.; Bottomley, L. A.; Brace, J. G.; Winograd, N. J. *J. Am. Chem. Soc.* **1980**, *102*, 4341.
(9) Bottomley, L. A.; Garrett, B. B. *Inorg. Chem.* **1982**, *21*, 1260.
(10) Schick, G. A.; Findsen, E. W.; Bocian, D. F. *Inorg. Chem.* **1982**, *21*, 2885.
(11) Schick, G. A.; Bocian, D. F. *J. Am. Chem. Soc.* **1983**, *105*, 1830.
(12) Tatsumi, K.; Hoffman, R. J. *J. Am. Chem. Soc.* **1981**, *103*, 3328.
(13) Mansuy, D.; Lecomte, J.-P.; Chottard, J.-C.; Bartoli, J.-F. *Inorg. Chem.* **1981**, *20*, 3119.
(14) Goedken, V. L.; Deakin, M. R.; Bottomley, L. A. *J. Chem. Soc., Chem. Commun.* **1982**, 607.
(15) Battioni, J.-P.; Lexa, D.; Mansuy, D.; Savéant, J.-M. *J. Am. Chem. Soc.* **1983**, *105*, 207.
(16) English, D. R.; Hendrickson, D. N.; Suslick, K. S. *Inorg. Chem.* **1983**, *22*, 367.
(17) Kadish, K. M.; Larson, G.; Lexa, D.; Momenteau, M. *J. Am. Chem. Soc.* **1975**, *97*, 282.

0020-1669/84/1323-3942$01.50/0

trido,[6-8] and μ-carbido iron porphyrin dimers. The first two complexes may be reduced in two steps or oxidized in four reversible, single-electron-transfer steps. For the case of the μ-carbido dimer, reduction to $[((TPP)Fe)_2C]^-$ and $[((TPP)Fe)_2C]^{2-}$ has also been shown[15] but no data have yet been presented on the multiple electrooxidation steps of this complex.

In this paper we demonstrate that $((TPP)Fe)_2C$ may be oxidized in four, single-electron-transfer steps to yield $[((TPP)Fe)_2C]^{4+}$. These electrode processes were investigated in six solvents including CH_2Cl_2/pyridine mixtures. In addition, formation constants were determined for the stepwise binding of pyridine by the neutral form as well as the singly and doubly oxidized forms of $((TPP)Fe)_2C$ in CH_2Cl_2.

Experimental Section

Materials. $((TPP)Fe)_2C$ was synthesized from (TPP)FeCl by using a modified synthetic method of Mansuy and co-workers[13] (since their use of iron powder as a reducing agent yielded some demetalation of the porphyrin). Typically, 500 mg of (TPP)FeCl was dissolved in 30 mL of anaerobic CH_2Cl_2. A large excess (500 mg) of $NaBH_4$ was added to this mixture under argon. Then 3 mL of anaerobic CH_3OH was added to solution, and the reduction of (TPP)FeCl to (TPP)Fe immediately occurred, yielding a red solution to which was added, under anaerobic conditions, 360 mg of freshly prepared CI_4.[19] The reaction was then allowed to occur under constant stirring for 2 h. Afterward the solution was washed with water, dried over Na_2SO_4, and evaporated, leaving dark purple crystals of crude $((TPP)Fe)_2C$, which were recrystallized from toluene/hexane (350 mg, yield $\simeq$75%). The purity of the product was ascertained by TLC on neutral alumina, UV–visible spectroscopy, and NMR spectrometry.

All solvents were purchased as reagent grade quality. Dichloromethane (CH_2Cl_2) and benzonitrile (PhCN) were distilled from P_2O_5. Tetrahydrofuran (THF) was purified via published methods[20] to remove peroxides. Pyridine (py) was distilled from KOH under inert atmosphere. The supporting electrolytes tetra-*n*-butylammonium perchlorate (TBAP) and tetra-*n*-butylammonium hexafluorophosphate ($(TBA)PF_6$) were obtained from Eastman Chemical Co. or Fluka Co. These salts were recrystallized from ethanol, dried in vacuo at 40 and 100 °C, respectively, and stored in a desiccator.

Instrumentation. Cyclic voltammetry experiments, with scan rates lower than 0.50 V/s, were carried out with either a Princeton Applied Research Model 174 A potentiostat, a Bioanalytical Systems Model CV-1B, or an IBM Instruments Model EC225 voltammetric analyzer. Current–voltage curves were recorded on a Houston Instruments Model 2000 X-Y recorder. For scan rates higher than 0.50 V/s, a PAR Model 173 potentiostat and Model 175 universal programmer or an IBM Instruments Model EC225 voltammetric analyzer was used, and current–voltage traces were recorded on a Tektronix Model 5111 oscilloscope coupled with a Tektronix C5A camera. A three-electrode system was used with a Pt-button working electrode, a Pt wire counterelectrode, and a saturated calomel electrode (SCE) as a reference electrode. To minimize aqueous contamination, the reference electrode was separated from the bulk of the solution by a cracked-glass bridge filled with the solvent plus supporting electrolyte. All solutions were deoxygenated by passing a stream of solvent-saturated prepurified N_2 for 10 min prior to recording voltammograms. All potentials reported are referred to the SCE and are good to ±10 mV.

Bulk electrolyses were carried out in a three-compartment cell. The working electrode and counterelectrode were large Pt grids, separated by a fritted-glass frit. Potentials were regulated by a PAR Model 173 potentiostat/galvanostat and Model 178 electrometer probe. Both the current and the total coulombs were monitored with a PAR Model 179 plug-in coulometer. Current–time curves were recorded on a Shimadzu Model R-12 strip chart recorder. Product appearance was monitored with UV–visible spectroscopy, by means of a UV–visible cell (path length 2.0 mm) attached to the electrolysis cell. A Tracor Northern Model 1710 holographic optical spectrometer/multichannel analyzer was used for all UV–visible measurements. Spectra from 290 to 920 nm resulted from the signal averaging of a minimum of 50 sequential spectral acquisitions. Spectral resolution was 1.2 nm.

Spectroelectrochemical experiments were also performed at an optically transparent thin-layer gold electrode (OTTLE) that consisted of a 100-lpi gold minigrid sandwiched between two glass slides, with a typical width of 0.10 mm.[21] Potentials were monitored with a PAR Model 173 potentiostat/galvanostat or an IBM Instruments Model EC225 analyzer. Scan rates were maintained below 7 mV/s. Because of high resistances inherent to the cell design, concentrations of supporting electrolytes were between 0.3 M in solvents of high dielectric constant and 0.5 M in solvents of lower dielectric constant.

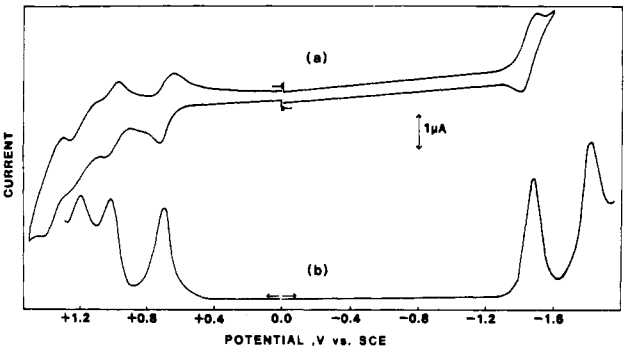

Figure 1. (a) Cyclic voltammogram and (b) differential-pulse voltammogram of 8.0×10^{-4} M $((TPP)Fe)_2C$ in CH_2Cl_2/0.1 M TBAP (modulation amplitude 25 mV). Scan rates: (a) 0.10 V/s; (b) 0.005 V/s.

Table I. Half-Wave Potentials for the Electron-Transfer Reactions of $((TPP)Fe)_2C$ in Selected Nonaqueous Solvents

	$E_{1/2}$, V vs. SCE					
solvent	4+/3+	3+/2+	2+/+	+/0	0/−	−/2−
CH_2Cl_2	+1.38	+1.17	+1.00	+0.67	−1.43	−1.82
PhCN		+1.25	+1.02	+0.67	−1.41	−1.74
THF				+0.86	−1.32	−1.56
DMF			+1.19	+0.54	−1.30[a]	−1.70[a]
py			+1.03	+0.52	−1.52	−1.77

[a] From ref 15.

Results and Discussion

Electrochemistry in Nonbinding Solvents. A typical cyclic voltammogram of $((TPP)Fe)_2C$ in CH_2Cl_2/0.1 M TBAP is shown in Figure 1. Six single-electron-transfer processes were observed between +1.60 and −1.90 V vs. SCE. These reactions are represented by eq 1–6, and half-wave potentials are listed in Table I.

$$((TPP)Fe)_2C + e^- \rightleftarrows [((TPP)Fe)_2C]^- \quad (1)$$

$$[((TPP)Fe)_2C]^- + e^- \rightleftarrows [((TPP)Fe)_2C]^{2-} \quad (2)$$

$$((TPP)Fe)_2C \rightleftarrows [((TPP)Fe)_2C]^+ + e^- \quad (3)$$

$$[((TPP)Fe)_2C]^+ \rightleftarrows [((TPP)Fe)_2C]^{2+} + e^- \quad (4)$$

$$[((TPP)Fe)_2C]^{2+} \rightleftarrows [((TPP)Fe)_2C]^{3+} + e^- \quad (5)$$

$$[((TPP)Fe)_2C]^{3+} \rightleftarrows [((TPP)Fe)_2C]^{4+} + e^- \quad (6)$$

Half-wave potentials for reactions 1 and 2 were also measured by classical polarography at the DME and differential-pulse voltammetry at a platinum electrode and gave results identical with cyclic voltammetric measurements.

Analysis of reaction 1 in PhCN indicated a peak separation of 70 mV at low scan rates, but i_{pa}/i_{pc} ratios were lower than 0.85 at scan rates below 0.1 V/s, thus suggesting a quasi-reversible electron transfer followed by a chemical reaction.[22] The presence of a chemical reaction following electron transfer

(18) Chang, D.; Cocolios, P.; Wu, Y. T.; Kadish, K. M. *Inorg. Chem.* **1984**, *23*, 1629.
(19) Soroos, H.; Hinkemp, J. B. *J. Am. Chem. Soc.* **1945**, *67*, 1642.
(20) Perrin, D. D.; Armarego, W. F. F.; Perrin, D. R. "Purification of Laboratory Chemicals", 2nd ed.; Pergamon Press: Oxford, 1980.
(21) Rhodes, R. K.; Kadish, K. M. *Anal. Chem.* **1981**, *53*, 1539.
(22) Nicholson, R. S.; Shain, I. *Anal. Chem.* **1964**, *36*, 706.

Table II. Spectral Properties of Oxidized and Reduced $((TPP)Fe)_2C$

species	solvent	λ_{max}, nm ($10^{-3}\epsilon$)				
$((TPP)Fe)_2C$	PhCN	400 (260)		530 (20)		
	CH_2Cl_2	398 (260)		529 (19)		
	DMF[a]	399 (370)		525 (19)		
$[((TPP)Fe)_2C]^-$	PhCN	406 (240)		529 (18)	605 (5)	
	DMF[a]	402 (330)		523 (28)	605 (15)	660 (sh)
$((TPP)Fe)_2C(py)$	py/CH_2Cl_2	402 (200)	411 (sh)	527 (15)	554 (sh)	
$((TPP)Fe)_2C(py)_2$	py	414 (230)		530 (15)	557 (12)	
b	py/benzene	418 (300)		532 (12)	560 (11)	

[a] Taken from ref 15, Figure 9. [b] The species is identified in ref 13 as a new complex produced by addition of py to $((TPP)Fe)_2C$ in benzene. On the basis of the data in this study, it appears that the bis(pyridine) complex has been produced.

was confirmed by thin-layer spectroelectrochemistry. Attempts to generate the $[((TPP)Fe)_2C]^-$ monoanion at a thin-layer electrode greatly depended on the supporting electrolyte utilized. With TBAP the electrogenerated $[((TPP)Fe)_2C]^-$ was stable for electrolysis times shorter than 25 s and then yielded monomeric $[(TPP)Fe]^-$ after cleavage of the dimer and addition of a second electron (reaction 7). The stability of the

$$((TPP)Fe)_2C \overset{e^-}{\rightleftharpoons} [((TPP)Fe)_2C]^- \xrightarrow{e^-} 2[(TPP)Fe]^- \quad (7)$$

singly reduced dimer in PhCN/0.3 M $TBA(PF_6)$ is illustrated by the thin-layer cyclic voltammogram shown in Figure 2a. The peak current ratio, i_{pa}/i_{pc}, is 1.0, and the reversibility of the reaction was confirmed by thin-layer controlled potential electrolysis. Furthermore, spectral monitoring of this electron-transfer process is illustrated in Figure 2b, and indicates that $[((TPP)Fe)_2C]^-$ does not decompose in PhCN/0.3 M $TBA(PF_6)$ for times as long as 90 s. Finally, reoxidation of $[((TPP)Fe)_2C]^-$ at −1.00 V quantitatively regenerated the initial spectrum. Maximum absorption wavelengths for this complex are summarized in Table II. Both the Soret and visible bands are very similar to those of the neutral $((TPP)Fe)_2C$ complex and no absorption is indicated above 650 nm. This suggests a strong charge localization within the Fe–C–Fe moiety.

The second reduction of $((TPP)Fe)_2C$ has been described in DMF as a quasi-reversible electron-transfer reaction followed by a very fast chemical step.[15] In this study, analyses of polarograms at a dropping-mercury electrode (in CH_2Cl_2) or cyclic voltammograms at a Pt electrode (in PhCN) yield similar conclusions. At a thin-layer electrode, in PhCN/0.3 M $(TBA)PF_6$, applying a potential of −2.0 V resulted in the irreversible appearance of a radical anion. This complex was oxidized by multiple waves on the reverse scan and has not been further identified.

Analysis of the current–voltage curves for the first oxidation (reaction 3) showed that the half-wave potential was independent of scan rate in a scan range of 0.010–1.0 V/s, while the anodic peak current was proportional to the square root of the scan rate. The ratio of the peak currents, i_{pc}/i_{pa}, was smaller than unity at scan rates between 0.02 and 0.10 V/s but approached a limit of 1.0 at all higher values of sweep rates. These data indicate that the first oxidation of $((TPP)Fe)_2C$ is electrochemically reversible but that the generated $[((TPP)Fe)_2C]^+$ cation undergoes a rapid chemical reaction. This reaction appears to involve a combination of dimer cleavage and carbon migration similar to that reported for $((TPP)Fe(C{=}C(p\text{-}ClC_6H_4)_2)$.[23,24] Detailed studies of this reaction are still in progress, and for this present paper, we will limit our discussions to oxidative voltammograms obtained at scan rates greater than 0.10 V/s. Under these conditions

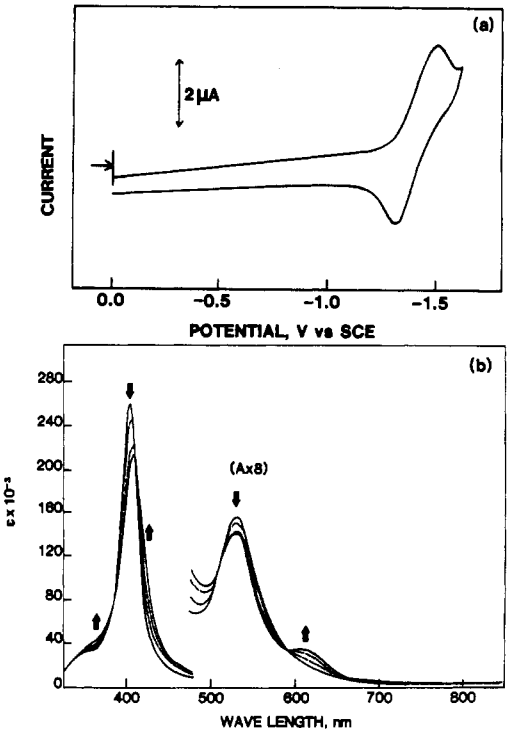

Figure 2. (a) Thin-layer cyclic voltammogram illustrating the reduction of 5.0×10^{-4} M $((TPP)Fe)_2C$ in PhCN/0.3 M $(TBA)PF_6$ (scan rate 3 mV/s). (b) Time-resolved electronic absorption spectra, taken at an OTTLE during the reduction of 5.0×10^{-4} M $((TPP)Fe)_2C$ in PhCN/0.3 M $(TBA)PF_6$.

minimal "interference" is observed due to the chemical reaction following charge transfer.

Current–voltage curves were analyzed for reactions 4–6 and indicated diffusion-controlled single-electron transfers. The currents for these reactions were partially overlapped by cyclic voltammetry ($E_{1/2}$ = 1.00, 1.17, and 1.38 V) but gave better resoltuion by differential-pulse voltammetry (see Figure 1b). Half-wave potentials (by cyclic voltammetry) were found to be independent of scan rate, and peak separations ($E_{pa} - E_{pc}$) were 60–70 mV at 0.10 V/s. In addition, all currents were proportional to the square root of scan rate above 0.10 V/s. These analyses are consistent with reversible to quasi-reversible electron transfers.[22]

Electrochemistry in py/CH_2Cl_2 Mixtures. A typical series of cyclic voltammograms in py/CH_2Cl_2/0.1 M TBAP is shown in Figure 3. Only the first reduction (reaction I) and the first two oxidations (reactions II and III) were monitored since pyridine is oxidized at potentials more positive than 1.0 V in CH_2Cl_2. As seen in Figure 3b, addition of 6.2×10^{-3} M py (10 equiv of py) to CH_2Cl_2 solutions produces a significant (200 mV) shift of $E_{1/2}$ for reaction II. This is consistent with a large stabilization of the singly oxidized complex by pyridine binding and also suggests a large formation constant for this reaction.[25-28] At 6.2×10^{-3} M py, half-wave potentials for

(23) Latos-Grazynski, L.; Cheng, R.-J.; La Mar, G. N.; Balch, A. L. *J. Am. Chem. Soc.* **1981**, *103*, 4270.
(24) Mansuy, D.; Morgenstern-Badarau, I.; Lange, M.; Gans, P. *Inorg. Chem.* **1982**, *21*, 1427.

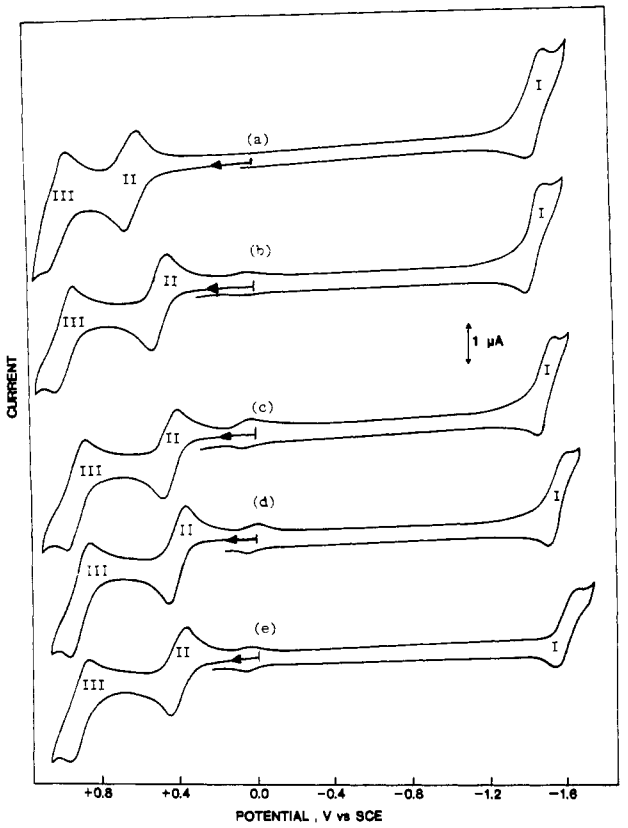

Figure 3. Cyclic voltammograms of 6.3×10^{-4} M $((TPP)Fe)_2C$ in py/CH_2Cl_2 mixed solvents, containing 0.1 M TBAP (scan rate 0.10 V/s). Pyridine concentrations: (a) 0; (b) 6.2×10^{-3} M; (c) 9.8×10^{-2} M; (d) 0.35 M; (e) 1.41 M.

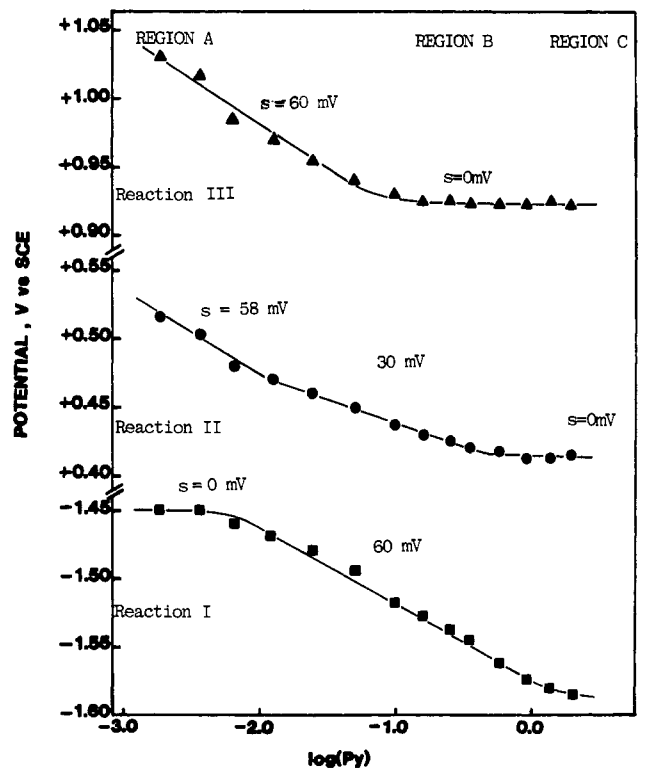

Figure 4. $E_{1/2}$ dependence on [py] for reactions I–III in Figure 3.

reactions I and III were identical with those in neat CH_2Cl_2. However, further increases in [py] produced negative shifts

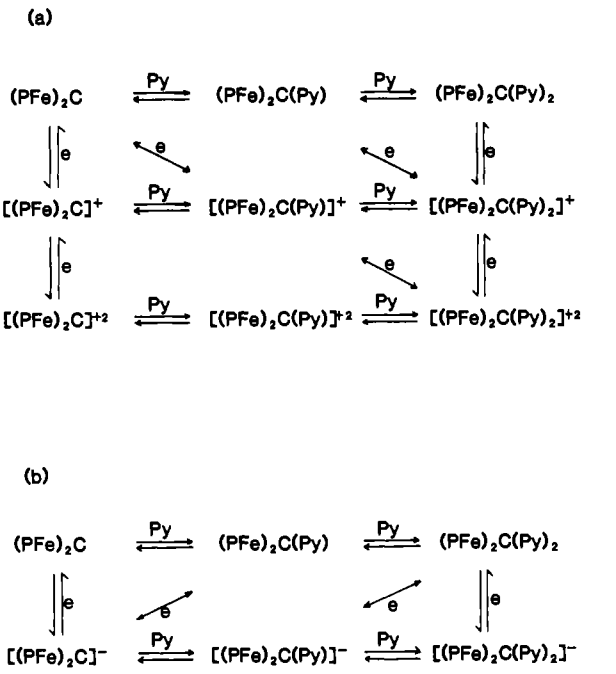

Figure 5. Schematic illustrations of electron-transfer and ligand-addition reactions of (a) oxidized and (b) reduced $((TPP)Fe)_2C$.

in all three waves as seen by the cyclic voltammograms of Figure 3c–e and, more clearly, by the plot of $E_{1/2}$ vs. log [py] shown in Figure 4. This latter plot is divided into three regions that are defined on the basis of the slopes of $E_{1/2}$ vs. log [py].

At low pyridine concentrations (region A), $E_{1/2}$ for reactions II and III shift by 59 ± 1 mV per tenfold increase in [py] while the half-wave potential for reaction I remains constant at $E_{1/2} = -1.45$ V. This dependence of $E_{1/2}$ on [py] is consistent with nonligated $((TPP)Fe)_2C$ and $[((TPP)Fe)_2C]^-$ (eq 1) but suggests that one py ligand is bound to $[((TPP)Fe)_2C]^+$, while two py ligands are bound to $[((TPP)Fe)_2C]^{2+}$. In this case the electrode reactions in region A (and Figure 3c) are represented by eq 8.

$$((TPP)Fe)_2C \underset{e^-}{\overset{py}{\rightleftharpoons}} [((TPP)Fe)_2C(py)]^+ \underset{e^-}{\overset{py}{\rightleftharpoons}} [((TPP)Fe)_2C(py)_2]^{2+} \quad (8)$$

In region B, the half-wave potential for reaction III remains constant at $E_{1/2} = +0.92$ V, while the measured $E_{1/2}$ for reactions I and II shifts cathodically by 60 and 35 mV, respectively, per tenfold increase in [py]. These shifts suggest the electrode reactions (9) and (10). Finally, in region C,

$$((TPP)Fe)_2C(py) \underset{e^-}{\overset{py}{\rightleftharpoons}} \left\{ \begin{array}{c} [((TPP)Fe)_2C(py)]^+ \\ \updownarrow \\ [((TPP)Fe)_2C(py)_2]^+ \end{array} \right\} \underset{e^-}{\overset{py}{\rightleftharpoons}} [((TPP)Fe)_2C(py)_2]^{2+} \quad (9)$$

$$((TPP)Fe)_2C(py) \underset{py}{\overset{e^-}{\rightleftharpoons}} [((TPP)Fe)_2C]^- \quad (10)$$

the half-wave potentials for reactions II and III remain constant at $E_{1/2} = +0.42$ V and $E_{1/2} = +0.92$ V, respectively. On the other hand, the half-wave potential for reaction I shifts

(25) Kadish, K. M.; Bottomley, L. A. *Inorg. Chem.* **1980**, *19*, 832.
(26) Walker, F. A.; Barry, J. A.; Balke, V. L.; McDermott, G. A.; Wu, M. Z.; Linde, P. F. *Adv. Chem. Ser.* **1981**, *No. 201*, 377.
(27) Kadish, K. M.; Bottomley, L. A.; Beroiz, D. *Inorg. Chem.* **1978**, *17*, 1124.
(28) Kadish, K. M. In "Iron Porphyrins"; Lever, A. B. P., Gray, H. B., Eds.; Addison Wesley: Reading, MA, 1982; Part 2, pp 161–249.

Table III. Formation Constants for py Addition to Oxidized and Reduced ((TPP)Fe)$_2$C Complexes in py/PhCN Mixtures[a]

formn const	$[((TPP)Fe)_2C]^{2+}$	$[((TPP)Fe)_2C]^{+}$	$((TPP)Fe)_2C$	$[((TPP)Fe)_2C]^{-}$
$\log K_1$		5.4 ± 0.2	2.3 ± 0.2 1.9 ± 0.2[b]	0.3 ± 0.3
$\log K_2$		1.0 ± 0.2	0.3 ± 0.2	$<10^{-2}$
$\log \beta_2$	7.7 ± 0.4	6.4 ± 0.4	2.6 ± 0.4	

[a] Except where indicated, values were calculated from electrochemical titration data. [b] Calculated from spectrophotometric titration data.

cathodically by less than 40 mV. This can be represented by eq 11 and 12. Combination of eq 1, 3, and 4 in CH_2Cl_2 with

$$((TPP)Fe)_2C(py)_2 \underset{e^-}{\rightleftharpoons} [((TPP)Fe)_2C(py)_2]^+ \underset{e^-}{\rightleftharpoons} [((TPP)Fe)_2C(py)_2]^{2+} \quad (11)$$

$$((TPP)Fe)_2(py)_2 \underset{py}{\overset{e^-}{\rightleftharpoons}} \begin{Bmatrix} [((TPP)Fe)_2C(py)]^- \\ \updownarrow \\ [((TPP)Fe)_2C(py)_2]^- \end{Bmatrix} \quad (12)$$

eq 8–12 in py/CH_2Cl_2 mixtures thus leads to the overall oxidation–reduction mechanism shown in Figure 5. This scheme is internally consistent with the observed electrochemical behavior and leads to an easy calculation of formation constants for ligand binding by the oxidized and reduced ((TPP)Fe)$_2$C complexes.

Formation Constants for py Addition to ((TPP)Fe)$_2$C. The addition of a single py ligand to ((TPP)Fe)$_2$C has been described in benzene[13] and a formation constant of log K^0 = 1.88 calculated for reaction 13. We have confirmed this reaction

$$((TPP)Fe)_2C + py \overset{K_1^0}{\rightleftharpoons} ((TPP)Fe)_2C(py) \quad (13)$$

in CH_2Cl_2/0.1 M TBAP but also see evidence for addition of a second ligand as shown by eq 14. This is illustrated in

$$((TPP)Fe)_2C(py) + py \overset{K_2^0}{\rightleftharpoons} ((TPP)Fe)_2C(py)_2 \quad (14)$$

Figure 6, which shows the UV–visible spectra at various py concentrations, and in Figure 7 by a plot of log $[(A_\infty - A)/(A - A_0)]$. As can be seen in Figure 6, two series of isosbestic points define two successive equilibria corresponding to reactions 13 and 14. Benesi–Hildebrand plots using the spectra of the initial two species gave slopes of 1.0 (Figure 7) and a formation constant of log K_1^0 = 1.9 ± 0.2. This is in agreement with literature data in benzene[13] and, as will be seen in the following section, also agrees with a value calculated from the half-wave potential dependence on [py]. No calculations could be performed for K_2^0 (reaction 14) since this second ligand addition reaction was not complete even at 6.0 M py.

Formation Constants for py Addition to Oxidized and Reduced ((TPP)Fe)$_2$C. Stepwise complexation of py is represented by eq 13 and 14 for the neutral ((TPP)Fe)$_2$C complex and by eq 15–17 for the oxidized and reduced complexes of

$$[((TPP)Fe)_2C]^+ + py \overset{K_1^+}{\rightleftharpoons} [((TPP)Fe)_2C(py)]^+ \overset{K_2^+}{\rightleftharpoons} [((TPP)Fe)_2C(py)_2]^+ \quad (15)$$

$$[((TPP)Fe)_2C]^{2+} + py \overset{K_1^{2+}}{\rightleftharpoons} [((TPP)Fe)_2C(py)]^{2+} \overset{K_2^{2+}}{\rightleftharpoons} [((TPP)Fe)_2C(py)_2]^{2+} \quad (16)$$

$$[((TPP)Fe)_2C]^- + py \overset{K_1^-}{\rightleftharpoons} [((TPP)Fe)_2C(py)]^- \overset{K_2^-}{\rightleftharpoons} [((TPP)Fe)_2C(py)_2]^- \quad (17)$$

((TPP)Fe)$_2$C. A value of K_1^0 for reaction 13 was calculated from the spectrophotometric titrations (see above section) and was also determined from the shift of half-wave potentials for reaction II in region A. This method of calculation has been described in the literature[25–28] and utilizes the type of data illustrated in Figure 4.

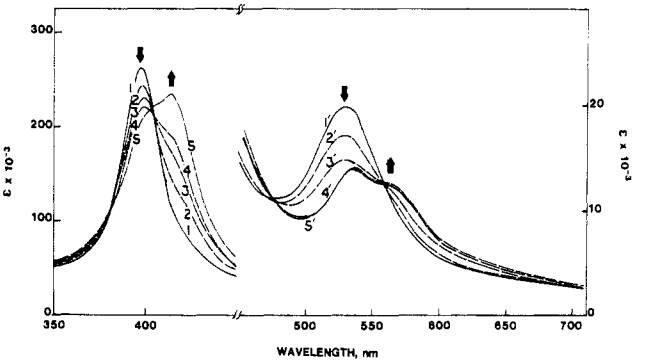

Figure 6. Electronic absorption spectra of ((TPP)Fe)$_2$C during a titration by py, in CH_2Cl_2/0.1 M TBAP. For the Soret region, $[((TPP)Fe)_2C] = 2.6 \times 10^{-5}$ M and [py] = (1) 0, (2) 1.2×10^{-3} M, (3) 9.1×10^{-3} M, (4) 4.8×10^{-2} M, and (5) 0.29 M. For the visible region, $[((TPP)Fe)_2C] = 4.9 \times 10^{-5}$ M and [py] = (1′) 0, (2′) 1.0×10^{-2} M, (3′) 5.0×10^{-2} M, (4′) 0.5 M, and (5′) 11.9 M.

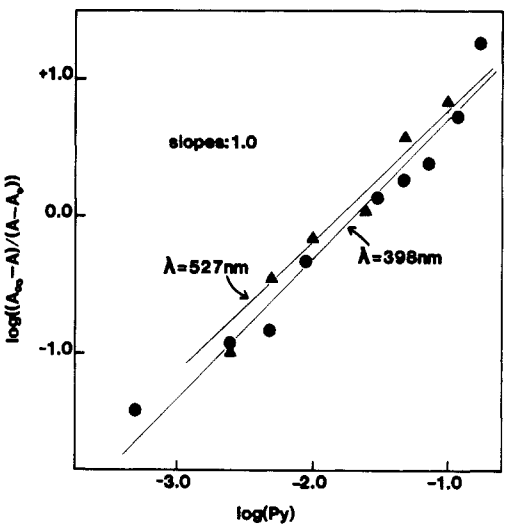

Figure 7. Log–log plot used in the calculation of K_1^0 for addition of py to ((TPP)Fe)$_2$C according to reaction 13. The data for this plot were taken from Figure 6.

Calculation of the first py addition to ((TPP)Fe)$_2$C according to reaction 13 gave log K_1^0 = 2.3 ± 0.2 by electrochemical techniques. This value is within experimental error of that calculated by the spectrophotometric titration (log K_1^0 = 1.9 ± 0.2), further confirming the validity of this value. This stability constant was then utilized to calculate the remainder of the formation constants given by eq 15–17 and illustrated in Figure 5. These values are presented in Table III, which summarizes all of the measured formation constants for pyridine addition. For the case of $[((TPP)Fe)_2C]^{2+}$, only log β_2^{2+} could be calculated, suggesting that $K_2^{2+} >> K_1^{2+}$. This was not true for the other three oxidation states of the complexes where $K_2 << K_1$. For the specific case of ((TPP)Fe)$_2$C, log K_2^0 = 0.3 ± 0.2 (reaction 14) was calculated while for $[((TPP)Fe)_2C]^-$, log K_2^- (reaction 17) was less than 10^{-2}.

As seen from Table III, the total ligation ability (log β_2) of the μ-carbido dimer decreases along the following sequence: dication > cation > neutral > anion. This trend is not unexpected and is followed for a large number of other iron porphyrins.[28] This trend also predicts that there should be no interaction of py with $[((TPP)Fe)_2C]^{2-}$. This dianionic complex is isoelectronic with $((TPP)Fe)_2O$, which does not bind py under any conditions.

Great care must be taken in making comparisons between ligand binding properties of the μ-oxo, μ-nitrido, and μ-carbido dimers. One notable difference in these complexes (in addition to the overall oxidation state) is the out-of-plane distance of the iron atom. $((TPP)Fe)_2O$ has the most out-of-plane iron atom (0.50 Å),[29] while $((TPP)Fe)_2C$ has the smallest out-of-plane iron distance (0.26 Å).[14] $((TPP)Fe)_2N$ has the iron atom removed by 0.32 Å from the mean porphyrin plane,[3] which is closer to that of $((TPP)Fe)_2C$ than that of $((TPP)Fe)_2O$. However, it is clear that changes in iron out-of-plane distances will also occur upon the stepwise binding of the two axial pyridine ligands. Structural studies of mono- and bis(pyridine) adducts, when available, should help to clarify the magnitude of formation constants obtained in this study and might explain the reason for the favoring of a single ligand-binding reaction by $((TPP)Fe)_2C$.

Acknowledgment. The support of the National Institutes of Health is gratefully acknowledged (Grant GM 25172). We also acknowledge helpful discussions with Dr. Larry A. Bottomley.

Registry No. $((TPP)Fe)_2C$, 75249-87-5; $[((TPP)Fe)_2C(py)_2]^{2+}$, 92054-65-4; $[((TPP)Fe)_2C(py)_2]^{2+}$, 92054-66-5; $[((TPP)Fe)_2C]^-$, 83928-16-9; py, 110-86-1.

(29) Hoffman, A. B.; Collins, D. M.; Day, V. W.; Fleischer, E. B.; Srivastava, T. S.; Hoard, J. L. *J. Am. Chem. Soc.* **1972**, *94*, 3620.

Contribution from the Department of Chemistry, University of Houston, Houston, Texas 77004, Laboratoires de Chimie, LA au CNRS No. 321, Département de Recherche Fondamentale, Centre d'Etudes Nucléaires de Grenoble, F.38041 Grenoble Cedex, France, and Laboratoire d'Electrochimie et de Chimie Physique, ERA au CNRS No. 468, Université Louis Pasteur, F.67000 Strasbourg, France

Electrochemistry of Oxo- and Peroxotitanium(IV) Porphyrins. Mechanism of the Two-Electron Reduction of a η^2-Coordinated Peroxo Ligand

TADEUSZ MALINSKI,[1a,d] DANE CHANG,[1a] JEAN-MARC LATOUR,[1b] JEAN-CLAUDE MARCHON,*[1b] MAURICE GROSS,[1c] ALAIN GIRAUDEAU,[1c] and KARL M. KADISH*[1a]

Received April 26, 1984

The oxidation and reduction reactions of oxotitanium(IV) tetraphenylporphyrin, TiO(TPP), peroxotitanium(IV) tetraphenylporphyrin, $Ti(O_2)(TPP)$, and peroxotitanium(IV) octaethylporphyrin, $Ti(O_2)(OEP)$, in dichloromethane were investigated by electrochemical and spectroscopic techniques. Two one-electron oxidations and two one-electron reductions of the porphyrin ring were observed for TiO(TPP). Similar oxidations were found for $Ti(O_2)(TPP)$ and $Ti(O_2)(OEP)$. In addition, the peroxo complexes showed three reduction steps. The first reduction gives a porphyrin anion radical complex, which undergoes protonation by trace water followed by internal electron transfer to give a hydroperoxotitanium(III) porphyrin complex. The latter is then reduced at the porphyrin-ring system. Finally, internal transfer of two electrons cleaves the oxygen–oxygen bond of the coordinated hydroperoxide to give the oxotitanium(IV) porphyrin complex and hydroxide ion. The overall reaction is a two-electron reduction of the peroxo ligand in an ECEC mechanism. The oxotitanium(IV) complex that is obtained can be further reduced to the anion radical and the dianion of the porphyrin ring. Possible competing processes, which result in a substoichiometric reduction of the peroxo ligand, are surveyed.

Introduction

Studies of dioxygen complexes of transition-metal porphyrins are of intrinsic importance in providing a better understanding of the bonding and reactivity of the dioxygen ligand in biological systems.[2-4] The properties of synthetic cobalt(II)[5-7] and iron(II)[8,9] porphyrin oxygen carriers have been intensively investigated. Among first-row transition-metal complexes, dioxygen adducts have also been obtained with chromium(II),[10] manganese(II),[11,12] and titanium(III) porphyrins.[13]

Recently, some of the present investigators (University of Houston) reported electrochemical studies of the diperoxomolybdenum(VI) porphyrin complex, $Mo^{VI}(O_2)_2(TmTP)$[14] (where TmTP is 5,10,15,20-tetra-*m*-tolylporphinato). It was shown that reduction occurred at the central metal and not at the porphyrin ring. This provided the first example where a peroxo-bound metalloporphyrin could be reduced at the central metal without affecting the nature of the metal–oxygen bond. This inertness was not observed by some of the present authors (C.E.N. Grenoble) in preliminary studies of the peroxotitanium(IV) porphyrin complex, $Ti^{IV}(O_2)(TPP)$ (where TPP is 5,10,15,20-tetraphenylporphinato). It was reported[15] that $Ti(O_2)(TPP)$ is electrochemically reduced in a two-electron irreversible process to the corresponding oxo complex,

(1) (a) University of Houston. (b) Centre d'Etudes Nucléaires de Grenoble. (c) Université Louis Pasteur. (d) Present address: Department of Chemistry, Oakland University, Rochester, MI 48063.
(2) Basolo, F.; Hoffman, B. M.; Ibers, J. A. *Acc. Chem. Res.* **1975**, *8*, 384-392 and references therein.
(3) Collman, J. P. *Acc. Chem. Res.* **1977**, *10*, 265-272.
(4) Jones, R. D.; Summerville, D. A.; Basolo, F. *Chem. Rev.* **1978**, *78*, 139-179.
(5) Walker, F. A. *J. Am. Chem. Soc.* **1970**, *92*, 4235-4244.
(6) Stynes, D. V.; Stynes, H. C.; James, B. R.; Ibers, J. A. *J. Am. Chem. Soc.* **1973**, *95*, 1796-1801.
(7) Hoffman, B. M.; Petering, D. H. *Proc. Natl. Acad. Sci. U.S.A.* **1970**, *67*, 637-643.
(8) Collman, J. P.; Gagne, R. R.; Reed, C. A.; Halbert, T. R.; Lang, G.; Robinson, W. T. *J. Am. Chem. Soc.* **1975**, *97*, 1427-1439.
(9) James, B. R. In "The Porphyrins"; Dolphin, D., Ed.; Academic Press: New York, 1978; Vol. 5.
(10) Cheung, S. T.; Grimes, C. J.; Wong, J.; Reed, C. A. *J. Am. Chem. Soc.* **1976**, *98*, 5028-5030.
(11) Gonzales, B.; Kouba, J.; Yee, S.; Reed, C. A.; Kirner, J.; Scheidt, W. R. *J. Am. Chem. Soc.* **1975**, *97*, 3247-3249.
(12) Hoffmann, B. M.; Wechsler, C. J.; Basolo, F. *J. Am. Chem. Soc.* **1976**, *98*, 5473-5482.
(13) Latour, J.-M.; Marchon, J.-C.; Nakajima, M. *J. Am. Chem. Soc.* **1979**, *101*, 3974-3976.
(14) Kadish, K. M.; Chang, D.; Malinski, T.; Ledon, H. *Inorg. Chem.* **1983**, *22*, 3490-3492.
(15) Guilard, R.; Latour, J.-M.; Lecomte, C.; Marchon, J.-C.; Protas, J.; Ripoll, D. *Inorg. Chem.* **1978**, 17, 1225-1235.

0020-1669/84/1323-3947$01.50/0